sustainability

MDPI

Article

Use of the Box–Behnken Experimental Design for the Optimization of Orange II (Acid Orange 7) Adsorption on *Aloe vera*

María Isabel Aguilar *, Mercedes Lloréns, Juan Francisco Ortuño, Víctor Francisco Meseguer, Ana Belén Pérez-Marín and Alejandro Cases

Departamento de Ingeniería Química, Facultad de Química, Universidad de Murcia, Campus de Espinardo, 30100 Murcia, Spain; llorens@um.es (M.L.); jfortuno@um.es (J.F.O.); vzapata@um.es (V.F.M.); abelenpm@um.es (A.B.P.-M.); tecaguaumu@gmail.com (A.C.)

* Correspondence: maguilar@um.es; Tel.: +34-868887091

Abstract: Industrial wastewater effluents containing dyes are considered to pollute and be harmful to the environment. Among the various removal techniques, the adsorption process using low-cost adsorbents has been successfully used to remove pollutants. In this work, *Aloe vera* leaves (AVs) have been used as adsorbent for the removal of Orange II (O-II). A three-level three-factor Box–Behnken factorial design, including three replicates of center points, was applied to investigate the main parameters affecting the biosorption of O-II dye in aqueous solutions by AVs. The selected parameters were adsorbent dose, initial dye concentration, and contact time. The Box–Behnken experiment design has given a satisfactory result for the optimization of the adsorption process. The obtained value of R^2 (0.9993) shows that the quadratic response model adequately represents the relationship between each response and the chosen variables. The pH influences the adsorption capacity, obtaining at pH 2 the maximum adsorption capacity value. From the kinetic models studied, the one that best describes the adsorption of Orange II on *Aloe vera* is the Bangham model (ARE = 1.06%). The isotherm model that best represents the experimental data is the Toth model. The maximum adsorption capacity obtained by this model was 15.9 $mg \cdot g^{-1}$.

Keywords: Box–Behnken design; Acid Orange 7; adsorption; *Aloe vera*; dye removal

Citation: Aguilar, M.I.; Lloréns, M.; Ortuño, J.F.; Meseguer, V.F.; Pérez-Marín, A.B.; Cases, A. Use of the Box–Behnken Experimental Design for the Optimization of Orange II (Acid Orange 7) Adsorption on *Aloe vera*. *Sustainability* **2023**, *15*, 15727. https://doi.org/10.3390/su152215727

Academic Editors: Md Nahid Pervez, Dongqi Wang and Tao Jiang

Received: 5 October 2023
Revised: 27 October 2023
Accepted: 31 October 2023
Published: 8 November 2023

1. Introduction

Protecting and conserving water has become one of the most pressing global issues. The release of industrial waste plays a significant role in the contamination of these water resources. Many sectors, including paper, printing, textiles, leather, cosmetics, and plastics, make extensive use of dyes. The release of such waste into the environment without thorough dye removal can have adverse effects on aquatic life. These include reduced sunlight penetration into the water, increased consumption of dissolved oxygen, and aesthetic damage to the aquatic environment. In addition, certain dyes have been shown to have the potential to disrupt endocrine systems, thereby affecting the aquatic ecosystem [1]. It should be noted that several commercial dyes contain components with toxicity, mutagenicity, and teratogenicity [2,3].

These constituents have the potential to leach into freshwater reservoirs, posing a threat to human well-being. Their persistence, bioaccumulation, and synergistic interactions increase the risks they pose to the environment and human health [4]. Most dyes exhibit high water solubility and a remarkable degree of persistence, making them resistant to removal via conventional methods such as flocculation or biodegradation [5]. Water pollution is one of the most important threats affecting our ecosystem in various ways.

The presence of stable aromatic rings in the molecular composition of dyes is at the root of their non-biodegradable and hazardous properties. Even minute concentrations, as low as one part per million (ppm), have the potential to cause pollution [6].

It is estimated that more than 10,000 different dyes and pigments are used across various industries, with approximately 0.7 million tons of dyes synthesized worldwide each year [7]. To put this into perspective, it takes approximately 200 L of water to produce 1 kg of textiles, and an average-sized textile facility consumes approximately 1.6 million liters of water per day [8].

Several methods, including electrochemical oxidation [9], biological treatment [10], coagulation [11], photodegradation [12], and others [13–17], have been developed to treat water and wastewater containing dyes.

Among the various techniques available for pollutant removal, the adsorption process offers numerous advantages, including high efficiency, cost effectiveness, ease of design, and the absence of toxic by-products [18–24]. In the pursuit of environmental protection and sustainability, researchers have explored various biomaterials for the remediation of contaminated wastewater.

In this study, the dye Orange II (Acid Orange 7) is used as an adsorbate. Its limited biodegradability and the presence of a monoazo group make it an environmental and public health hazard. Therefore, its removal from water is imperative due to its toxicity.

The adsorbent widely used for the removal of a wide range of dyes is activated carbon. However, this material is costly and presents challenges in terms of regeneration [25]. Therefore, the search for alternative, inexpensive, and easily regenerated adsorbents has become imperative to make the adsorption process more feasible for wastewater treatment [26,27]. Recently, various materials, such as spent tea leaves [28], the Moringa peregrina plant [29], activated papaya leaves [30], corn leaves [31], and a variety of fruit peels including watermelon [32], mango [33], pomegranate [34], banana [35], dragon fruit [36], as well as leaf-based adsorbents [37], have demonstrated successful applications for the removal of dyes from aqueous solutions via adsorption.

Aloe vera leaves were selected as the adsorbent material for this study. *Aloe vera* is known for its significant role as a medicinal plant with multiple applications [38]. Apart from its use in medicine and pharmaceuticals, *Aloe vera* is also used in the food industry, cosmetics, and even nanotechnology [39–41]. Recently, there has been a growing interest in the use of *Aloe vera* and its derivatives for environmental purposes, particularly as an adsorbent for the removal of metals, dyes, and various pollutants from aqueous waste streams [42–45].

In order to investigate the main factors influencing the adsorption of the Orange II dye in aqueous solutions by *Aloe vera* leaves, a response surface methodology (RSM) based on a three-level three-factor Box–Behnken factorial design, with three replicates at the central points, has been used. BBD proves advantageous in preventing experiments from taking place under extreme conditions as it does not involve the highest- and lowest-level combinations for each factor [46]. It has been used to optimize various chemical and physical processes, with a number of experiments determined accordingly [47]. Additionally, it provides the advantage of not having to conduct experiments under conditions that, in some cases, are difficult to carry out due to the physical or economic limitations of the experimental process [48]. The main parameters affecting the efficiency of the adsorbent are initial adsorbate concentration, adsorbent dosage, pH, contact time, and temperature. Among the critical factors influencing dye removal by biosorption, we specifically focused the study on adsorbent dosage, initial dye concentration, and contact time to evaluate their combined effect on biosorption efficiency. These parameters were chosen due to their significant influence in other adsorption studies cited in the bibliography [42,49,50]. The effect of the pH of the solution is extremely important when the adsorbate is ionized as a function of the pH of the solution, as it is in the case of the dye used in this study. It is then interesting to consider the relationship between the chemical form of the adsorbate at the pH of the solution and the pH_{zpc} of the adsorbent during the adsorption process. So, preliminary tests were carried out to determine the influence of this factor on the adsorption uptake, and to establish the optimum pH at which to carry out the following tests and the

experimental design. Once the pH value was established, the influences of the other three factors were studied.

Aloe vera has traditionally been used in medicine and cosmetics, but its application in the environmental field is very recent and its use in water treatment is one of its most promising applications [44,51]. Its use as an adsorbent material for the elimination of certain pollutants present in water has been showing very interesting results, as it is an abundant material in nature and therefore inexpensive. In this work, *Aloe vera* was used for the removal of a dye (Orange II). It was decided that we would not to carry out *Aloe vera* activation treatment in order to not make the dye removal process more expensive. Furthermore, the Box–Behnken experimental design was used to optimize the study of the adsorption process and to find out the influences and interactions of the variables studied. *Aloe vera* was found to be a very promising material for use as an adsorbent in processes for the removal of pollutants from aqueous streams.

2. Materials and Methods

2.1. Biosorbent Preparation

For the preparation of the biosorbent [52], *Aloe vera* leaves were cut, washed with tap water, and subsequently cut up again. Next, the leaves were placed in an oven at 50 °C–60 °C and left to dry for a few days until they were free of moisture. Then, the obtained biomass was ground and sieved to a particle size of less than 1 mm. The sieved product was washed with distilled water under agitation, and then dried again in the oven (50 °C–60 °C), until the adsorbent solid was obtained completely dry (up to a constant weight) and with the required particle size.

2.2. Characterization of Biosorbent

To characterize the biosorbent, the total attenuated reflection Fourier transform infrared spectroscopy (ATR-FTIR) technique was used. To detect the presence of the functional groups responsible for the adsorption of O-II, a Nicolet™ iS™ 5 FTIR spectrometer from Thermo Scientific was employed.

Another parameter used for the characterization of the adsorbent solid was the pH of zero point charge (pH_{zpc}). To determine the pH_{zpc}, two methods were used: mass titrations and an immersion technique. In the former, a procedure like that described by Fiol and Villaescusa [53] was carried out. Different masses of solid adsorbent (2.5–80 $g \cdot L^{-1}$) were added into glass flasks containing 5 mL of 0.01 M NaCl solution. They were kept in agitation at 25 °C until the pH remained constant. In the immersion technique, 0.06 g of sorbent was added to flasks containing 20 mL of 0.01 M NaCl solution (with pH values from 3.1 to 12). The suspension was agitated at 25 °C until an equilibrium pH was achieved [42,53,54]. In both methods, once equilibrium was reached, the final pH of the suspension was determined.

2.3. Adsorbate

The Orange II (Acid Orange 7, C.I. 15110) was supplied by Sigma Aldrich. A stock solution of 1000 $mg \cdot L^{-1}$ Orange II at pH 2 was prepared, from which the different solutions used in the tests were obtained. A visible spectrophotometer (WPA Biochrom S1200, Biochrom Ltd., Cambridge, UK) was used to determine the concentration of Orange II dye in each solution. The measurements were made at a wavelength of 485 nm.

2.4. Design of Experiments—DOE

The design of experiments (DOE) was used to determine the influence of different variables on O-II biosorption removal, reducing the amount of experimental work that needed to be carried out for the adsorption studies [55].

In this research, a three-level three-factor Box–Behnken factorial design, including 3 replicates of the center points, was used to investigate the main parameters affecting the biosorption of O-II dye in aqueous solutions by AV.

Among the most important parameters that affect the removal of dyes by biosorption, adsorbent dose, initial dye concentration, and contact time were selected for evaluation of their combined effect on biosorption efficiency.

A total of 15 experiments were carried out. The adsorbent dose range studied was between 1 and 4 $g \cdot L^{-1}$, the initial dye concentration of the aqueous solutions varied between 10 and 50 $mg \cdot L^{-1}$, and the contact time was evaluated from 10 to 60 min. The pH was set at 2 given the nature of the dye and considering the preliminary tests carried out, in which it was found that the highest adsorption of Orange II occurred at this pH.

A quadratic response model was used to explain the relationships between the response and the factors considering the different terms, described by Equation (1):

$$Y = \beta_0 + \sum_{i=1}^{k} \beta_i X_i + \sum_{j=i}^{k} \beta_{jj} X_j^2 + \sum_{i=1}^{k} \sum_{j=1}^{k} \beta_{ij} X_i \quad (1)$$

where:

Y = predicted response values (dye adsorption capacity, q)
k = numbers of variables
β_0, β_i, β_{jj} and β_{ij} = intercept, quadratic, linear, and interaction effects, respectively
X_i, X_j = independent variables

2.5. Batch Adsorption Studies

A series of batch experiments were performed to investigate the influence of pH, study the kinetics of adsorption, and obtain the equilibrium isotherms. For each of the results obtained in the different experiments, the adsorption capacity (q, $mg \cdot g^{-1}$) was determined using Equation (2):

$$q = \frac{(C_0 - C) \cdot V}{m} \quad (2)$$

where:

C_0 = initial dye concentration in the solution ($mg \cdot L^{-1}$)
C = dye concentration in the solution at time t ($mg \cdot L^{-1}$)
V = solution volume (L)
m = adsorbent mass (g)

2.5.1. Influence of pH on Adsorption

To verify the influence of pH on adsorption, several tests were carried out at different pH values, keeping the initial concentration of Orange II constant. Two types of tests were performed. On the one hand, tests were carried out at different pH values, controlling the constancy of the pH value throughout the test duration by means of small additions of diluted solutions of NaOH or HNO_3. On the other hand, tests were carried out at different initial pH values in which the pH was not controlled throughout the process, and its value was measured at the end of the test.

The pH range studied was from 2 to 10. A total of 30 mL of a 50 $mg \cdot L^{-1}$ Orange II solution and 0.075 g of adsorbent solid were placed in 100 mL glass bottles. The assay was kept in a thermostatic bath at 25 °C, with magnetic stirring, until equilibrium was reached after approximately 6 h of contact. Once equilibrium was reached, the adsorbent solid was separated from the liquid by centrifugation and, after dilution, when it was necessary, the absorbance of the liquid was measured at 485 nm with the visible spectrophotometer.

2.5.2. Biosorption Kinetics

To study the adsorption kinetics, 80 mL of an Orange II solution with a concentration of 50 $mg \cdot L^{-1}$ at pH 2 was combined with 0.2 g of adsorbent solid and at a temperature of 25 °C. Samples were taken at different times and centrifuged to separate the solid as quickly as possible. After diluting, the supernatant, if necessary, the absorbance of the dilution was

measured in the spectrophotometer to determine the O-II concentration. The assay finished when equilibrium was reached (when the concentration of O-II in the supernatant solution remained constant).

In this research, different kinetic models described in the literature [52,55–57] were used to fit the experimental data in order to investigate the mechanisms involved in dye sorption on *Aloe vera* (Table 1).

Table 1. Kinetic models.

Kinetic Model	Equation	Parameters
Pseudo—first order	$q = q_e \cdot (1 - e^{-k_1 \cdot t})$	q_e, adsorption capacity at equilibrium
		k_1, adsorption rate constant
Pseudo—second order	$q = \frac{t}{\frac{1}{k_2 \cdot q_e^2} + \frac{t}{q_e}}$	q_e, adsorption capacity at equilibrium
		k_2, adsorption rate constant
		$h = k_2 \cdot q_e^2$, initial adsorption rate
Elovich equation	$q = \frac{1}{\beta} \cdot \ln(\alpha \cdot \beta) + \frac{1}{\beta} \cdot \ln t$	α, initial adsorption rate
		β, constant related to the extent of surface coverage and activation energy for chemisorption
Intraparticle diffusion	$q = k_d \cdot t^{1/2} + C$	k_d, rate constant
		C, constant related with the thickness of boundary layer
Bangham	$\log\left\{\log\left(\frac{C_0}{C_0 - q \cdot r}\right)\right\} = \log\left(\frac{k_B \cdot r}{2.303}\right) + \sigma \log(t)$	k_B, constant parameter
		σ, constant parameter (<1)

2.5.3. Biosorption Isotherms

To obtain the adsorption isotherms, O-II solutions were prepared at pH 2 and concentrations of 10, 20, 30, 40, 50, 60, 80, and 100 ($mg \cdot L^{-1}$). Then, 30 mL of each solution was placed in glass flasks (100 mL) and combined with 0.075 g of adsorbent (2.5 $g \cdot L^{-1}$ dose). It was then kept in a thermostatic bath at 25 °C with magnetic stirring until equilibrium was reached (≈6 h). Once this time had elapsed, samples were taken from the suspensions and centrifuged to separate the solid, and the absorbance of the sample was measured to determine the O-II concentration.

The most common isotherm models found in the bibliography [52,58–60] were used to explain the adsorption equilibrium; they can be found in Table 2.

Table 2. Isotherm models.

Isotherm Models	Equation	Parameter
Langmuir	$q_e = \frac{q_{mL} \cdot K_L \cdot C_e}{1 + K_L \cdot C_e}$	q_{mL}, maximum sorption capacity
		K_L, Langmuir isotherm constant
Freundlich	$q_e = K_F \cdot C_e^{1/n}$	K_F, Freundlich isotherm constant
		n, Freundlich isotherm exponent constant
Redlich–Peterson	$q_e = \frac{K_R \cdot C_e}{1 + \alpha_R \cdot C_e{}^{\beta}}$	K_R, Redlich–Peterson isotherm constant
		α_R, Redlich–Peterson isotherm constant
		β, Redlich–Peterson isotherm exponent
Sips	$q_e = \frac{q_{mS} \cdot K_S \cdot C_e{}^{1/n_S}}{1 + K_S \cdot C_e{}^{1/n_S}}$	q_{mS}, maximum sorption capacity
		K_S, Sips isotherm constant
		n_S, Sips isotherm exponent

Table 2. *Cont.*

Isotherm Models	Equation	Parameter
Toth	$q_e = \frac{q_{mT} \cdot K_T \cdot C_e}{(1+K_T \cdot C_e^{1/T_T})^{T_T}}$	q_{mT}, maximum sorption capacity
		K_T, constant that characterize the adsorptive potential
		T_T, Toth parameter related with the heterogeneity of the adsorbent (dimensionless)
Dubinin–Radushkevich	$q_e = q_{m_{DR}} e^{-K_{DR}\varepsilon^2}$	q_{mDR}, maximum sorption capacity
		K_{DR}, constant related to the adsorption energy
		ε, Polanyi potential, calculated from: $\varepsilon = RT \ln\left(1 + \frac{1}{C_e}\right)$

3. Results

3.1. Characterization of Aloe vera

The functional groups present on the biosorbent surface are the bases for understanding the binding mechanism of the dye to the solid. In order to identify the main functional groups present on the *Aloe vera* surface, an ATR-FTIR analysis was performed. The adsorption bands can be seen in the spectra from Figure 1, reflecting the complex nature of the adsorbent solid [42,61]. The presence of the absorption bands mentioned below are highlighted.

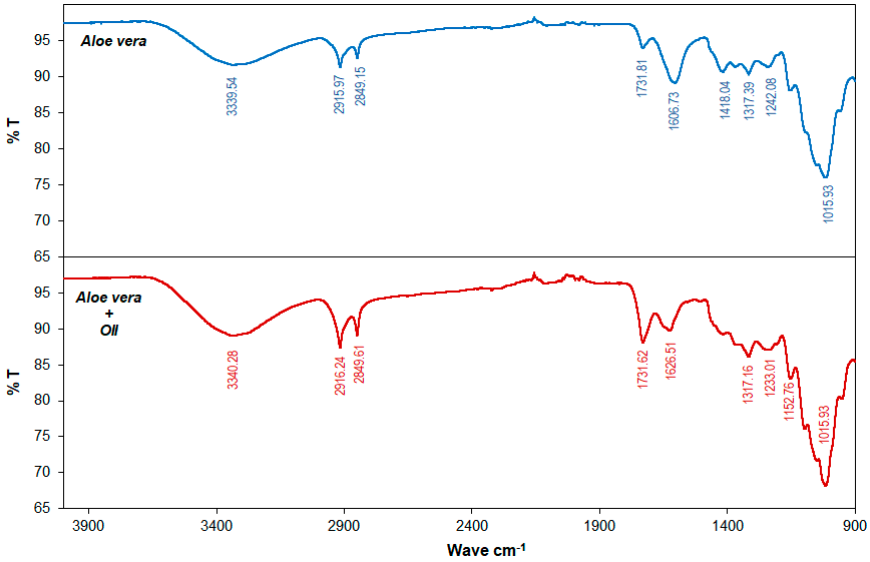

Figure 1. ATR-FTIR spectra of *Aloe vera* before and after biosorption of O-II. Spent adsorbent (AV+O-II) obtained: pH = 2, C_0 = 100 mg·L^{-1}, sorbent dose = 2.5 g·L^{-1}, contact time = 6 h.

The broad band around 3340 cm^{-1} could be attributed to free and hydrogen-bonded hydroxyl groups and phenolic –OH stretching frequency. Phenolic –OH group stretching is related to the presence of this group in diverse components of *Aloe vera*, such as flavonoids, flavonols, anthraquinones, etc. [62]. The peaks at 2916 cm^{-1} and 2849 cm^{-1} may be due to the stretching and bending vibrations of the C-H bond present in CH_2 groups [43,44]. The absorption peak at 1732 cm^{-1} could be assigned to the carbonyl group as a result of C=O stretching [44,45]. The bands shown at 1606 cm^{-1} and 1418 cm^{-1} can be assigned to the asymmetric and symmetric carboxyl C=O stretching group [43,44,62]. The peaks at about 1317 cm^{-1} and 1015 cm^{-1} could be due to the stretching vibrations of the C-O bond from different groups (carboxylic acid, alcoholic, phenolic, ether, or ester) [43]. El-Azazy et al. [45] attribute this last peak to C–O stretching due to the presence of rhamnogalacturonan, a

side-chain component of pectins. The two absorption peaks observed at 1242 cm^{-1} and 1153 cm^{-1} indicate the presence of C–C stretching and C–O–C stretching of the aliphatic ether, respectively [45].

These results are in agreement with the findings of various authors in the literature; furthermore, these functional groups are commonly present in plant constituents such as polysaccharides, lignin, proteins, anthraquinones, etc. [42,43,62].

Small variations in the intensity of the absorption peaks and slight changes in the wave number of the dominant peaks can help to attribute the participation of the different functional groups in dye biosorption. Therefore, the spectra of the biosorbent (*Aloe vera*) and that of *Aloe vera* loaded with Orange II were compared (Figure 1). A change in the transmittance percentage of some peaks can be seen, while in others, a slight shift in the wave number is observed, which suggests the possible groups involved during O-II biosorption onto *Aloe vera* [42,47,49,52,63,64].

The point of zero charge determined using the immersion technique was 4.5, while this value was around 4.1 when the mass titration technique was applied. This indicates that at pH < 4.1, the adsorbent solid is positively charged and electrostatic interactions can take place between the *Aloe vera* and dye [42,53,65].

In addition, the bibliography contains studies that include the characterization of *Aloe vera* using scanning electron microscopy (SEM), under conditions similar to those used in this study, which show the heterogeneous surface of the adsorbent containing numerous pores of different sizes [43,45]. Choi et al. (2016) [66] have carried out a fairly complete study of the surface structures of *Aloe vera*.

3.2. Box–Behnken Design

As mentioned in the Section 2, the parameters chosen in order to study their influence on O-II removal by biosorption were adsorbent dose, initial dye concentration, and contact time.

Table 3 shows the Box–Behnken experiment design matrix for the real and coded variables and the analyzed response (q = dye adsorption capacity).

Table 3. Box–Behnken design matrix for real and coded variables and the measured responses values.

Test	Coded Variable			Real Variable			Response
	X_1	X_2	X_3	X_1	X_2	X_3	
	Dose	[O-II]	Time	Dose ($g \cdot L^{-1}$)	[O-II] ($mg \cdot L^{-1}$)	Time (min)	q ($mg \cdot g^{-1}$)
1	−1	−1	0	1	10	35	5.29
2	1	−1	0	4	10	35	2.21
3	−1	1	0	1	50	35	8.45
4	1	1	0	4	50	35	6.78
5	−1	0	−1	1	30	10	7.14
6	1	0	−1	4	30	10	4.97
7	−1	0	1	1	30	60	7.98
8	1	0	1	4	30	60	5.43
9	0	−1	−1	2.5	10	10	3.01
10	0	1	−1	2.5	50	10	6.80
11	0	−1	1	2.5	10	60	3.31
12	0	1	1	2.5	50	60	7.78
13	0	0	0	2.5	30	35	6.53
14	0	0	0	2.5	30	35	6.58
15	0	0	0	2.5	30	35	6.53

A second-order polynomial equation with interaction terms was obtained using Minitab® 15 software that relates the studied responses to the chosen variables.

An analysis of the significance and adequacy of the quadratic regression model was performed for the coded variables because the use of these variables in the fitted model increases the accuracy of the estimation of model coefficients and enhances their interpretation [67]. The estimated coefficients in the model, and the *t*- and *p*-values for all linear, quadratic, and interaction effects of the parameters, are given in Table 4 for the adsorption capacity. Student's *t*-test and *p*-values can be used to assess the significance of the different terms in the regression model [50,68]. Normally, a higher *t*-value, and lower *p*-value, means that the coefficient term is significant [50]

Table 4. Estimated regression coefficient and corresponding *t*- and *p*-values for adsorption capacity.

Term	Coef	SE Coef	*t*	*p*
Constant	6.54843	0.04874	134.3680	0.0000
X_1	−1.18414	0.02984	−39.6780	0.0000
X_2	1.99931	0.02984	66.9920	0.0000
X_3	0.32172	0.02984	10.7800	0.0000
$X_1 \cdot X_1$	0.14376	0.04393	3.2730	0.0220
$X_2 \cdot X_2$	−1.01200	0.04393	−23.0370	0.0000
$X_3 \cdot X_3$	−0.31235	0.04393	−7.1100	0.0010
$X_1 \cdot X_2$	0.35243	0.04221	8.3500	0.0000
$X_1 \cdot X_3$	−0.09561	0.04221	−2.2650	0.0730
$X_2 \cdot X_3$	0.16723	0.04221	3.9620	0.0110

Additionally, to assess the effect of each factor and whether there are interactions between them, a Pareto analysis was performed [67,69]. For each factor, the percentage effect (P_i) on the response (q) was calculated using Equation (3) [69]:

$$P_i = \frac{\beta_i^2}{\sum_1^9 \beta_i^2} \cdot 100 \ (i \neq 0) \quad (3)$$

where β_i is the regression coefficient estimated for each variable. The Pareto chart analysis is shown in Figure 2, where bar length corresponds to the percentage effect of each factor.

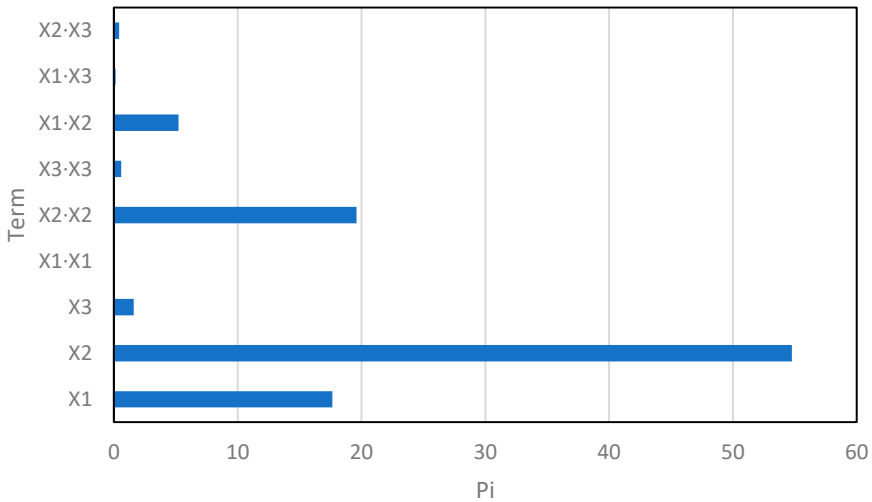

Figure 2. Pareto chart analysis for the Box–Behnken experiment design.

It was observed that the most significant factors on the adsorption capacity are X_2 (initial dye concentration) and X_1 (adsorbent dose), respectively. The value of P_i is 54.8% for X_2, 19.6% for $X_2{}^2$, and 17.6% for X_1, being 5.2% for the interaction of the two factors.

An evaluation of model fitting for the Box–Behnken experimental design can be carried out via analysis of variance (ANOVA) [46]. The results of this ANOVA, provided by Minitab, are shown in Table 5.

Table 5. Analysis of variance for q.

Source	Degrees of Freedom (DF)	Seq SS	Adj SS	Adj MS	F	*p*
Regression	9	48.8666	48.8666	5.4296	762.02	0.0000
Linear	3	44.0235	44.0235	14.6745	2059.49	0.0000
Square	3	4.1978	4.1978	13.9930	196.38	0.0000
Interaction	3	0.6452	0.6452	0.2151	30.19	0.0010
Residual error	5	0.0356	0.0356	0.0071		
Lack of fit	3	0.0342	0.0342	0.0114	16.31	0.0580
Pure error	2	0.0014	0.0014	0.0007		
Total	14	48.9023				

Taking into account the ANOVA results, the F values are high while *p*-values are lower ($p < 0.05$), which suggests that dye adsorption capacity can be predicted adequately by the regression equation obtained. The *p*-value for "lack of fit" being > 0.05 indicated that the lack of fit was not significant and that this regression model was valid for the O-II biosorption on *Aloe vera* [50,70].

The dye adsorption capacity (q) expressed in the function of the three factors studied as independent variables is given by Equation (4):

$$\begin{aligned} q(mg \cdot g^{-1}) \; = \; & 3.519 - 1.3271X_1 + 0.2107X_2 + 0.0442X_3 + 0.0639X_1^2 - 0.0025X_2^2 \\ & -4.998 \cdot 10^{-4}X_3^2 + 0.0118X_1 \cdot X_2 - 0.0026X_1 \cdot X_3 + 0.0003X_2 \cdot X_3 \end{aligned} \quad (4)$$

where:

X_1 = adsorbent dose, $g \cdot L^{-1}$

X_2 = initial dye concentration, $mg \cdot L^{-1}$

X_3 = contact time, min

The coefficient of the determination (R^2) value obtained (0.9993) determines that the model adequately represents the relationship between each response and the chosen variables. The high adjusted R^2 values (0.9980) show a high correlation between the observed and the predicted values. In addition, the predicted R^2 values (0.9887) suggest that the model can be used to predict new observations [47].

Figure 3 shows the experimental values versus the values estimated with the model for O-II adsorption capacity onto *Aloe vera*. As can be seen, there is a high degree of adjustment, which is also reflected by the high value of R^2.

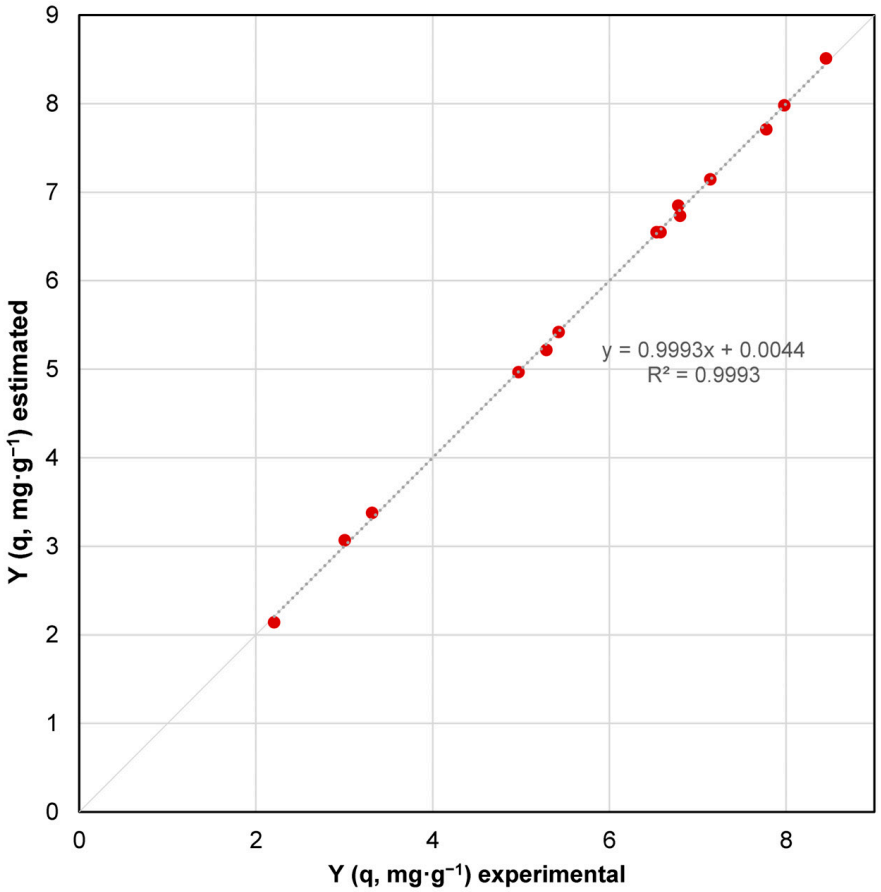

Figure 3. Model prediction of dye adsorption capacity versus experimental values.

3.2.1. Influence of Different Parameters Affecting the Biosorption of O-II dye by *Aloe vera*

A 3D response surface and contour graph for the dye adsorption capacity (Figure 4) were used as a graphical interpretation of the second order model equation to analyze the relationship between the amount of O-II adsorbed and the factors considered in the biosorption study.

3.2.2. Effects of Adsorbent Dose (D) and Initial O-II Concentration ($[O\text{-}II]_i$)

The effects of D and $[O\text{-}II]_i$ at a fixed time (35 min) on the dye adsorption capacity are represented in Figure 4a. The curvature of the response surface indicates the influence of the studied variables. It can be observed that the adsorption capacity increased with increases in the initial concentration of dye, while it decreased with increasing doses of the adsorbent. This last parameter affects the O-II adsorption capacity to a lesser extent. These results are consistent with those observed earlier in the Pareto chart analysis and with the significance attributed to these two factors.

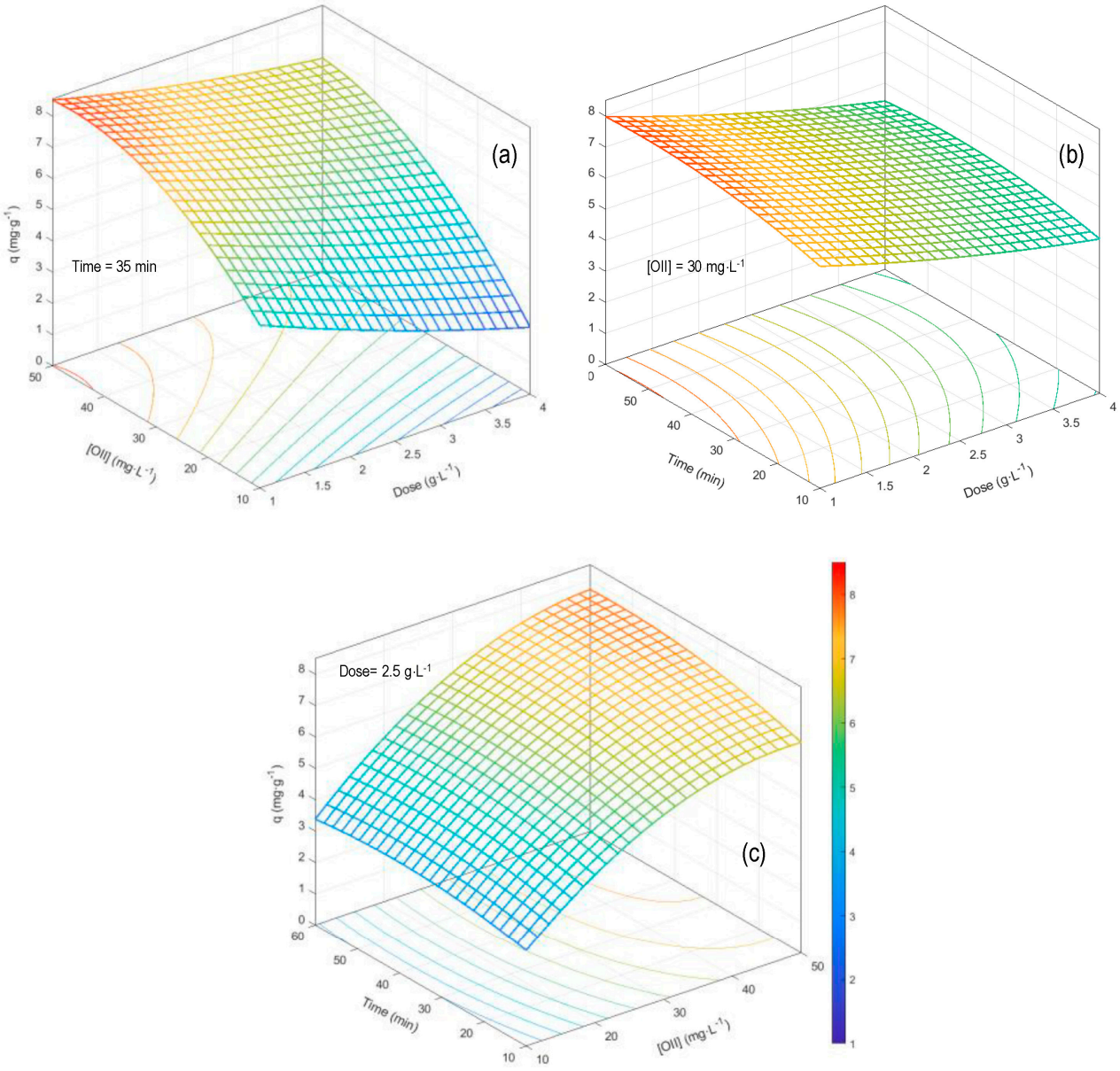

Figure 4. The 3D response surface and contour graph for dye adsorption capacity versus two of the different factors studied, holding the third factor constant as its central value. (**a**) Contact time constant (**b**) Initial O-II Concentration constant (**c**) Dose constant.

3.2.3. Effect of Adsorbent Dose (D) and Contact Time (t)

Figure 4b shows the influence of adsorbent dose and contact time on keeping the $[O\text{-}II]_i$ at 30 mg·L^{-1}. The slight curvature of the response surface indicates that there is little interaction between these parameters. The O-II adsorption capacity did not change significantly with contact time in the studied range (10 min to 60 min), probably because the adsorption kinetics are very fast.

3.2.4. Effect of Initial O-II Concentration ($[O\text{-}II]_i$) and Contact Time

The effects of initial O-II concentration and contact time were investigated while maintaining the adsorbent dose at 2.5 g·L^{-1} and the results are presented in Figure 4c, clearly showing that the O-II adsorption capacity increased with initial O-II concentration, while the influence of the contact time was not significant. The initial concentration of the dye is an important parameter in the adsorption process [64], as can be seen in Figure 4a;

the O-II adsorption uptake increased with initial dye concentration and began to stabilize from values of 40 mg·L^{-1}, which implies that the adsorption sites of the biosorbent were saturated and there were no more available binding sites for adsorption [49].

3.3. Effect of pH on O-II Biosorption

The influence of pH on biosorption is an important factor to consider since the pH value of the solution can affect the affinity between the surface of the biosorbent and the dye (adsorbate). This is because it can affect both the ionization of the adsorbate and the ionization of functional groups present on the surface of the adsorbent solid [71–73].

The effect of pH was studied in a series of batch experiments (pH range: 2–10). A series of pH controlled tests were performed and other experiments were carried out without pH control.

Figure 5a shows the pH of the dye solution before (initial) and after (final) contact with the biosorbent, in experiments performed with no pH control. It can be seen when the initial pH is 2 that there is no change in the final pH value, but for the rest of the initial pH values, changes can be observed in the pH value during the adsorption of O-II on *Aloe vera*. At pH 4 and 6, there are small variations, but at higher initial pH values, there is a considerable decrease in the final pH compared to the initial pH.

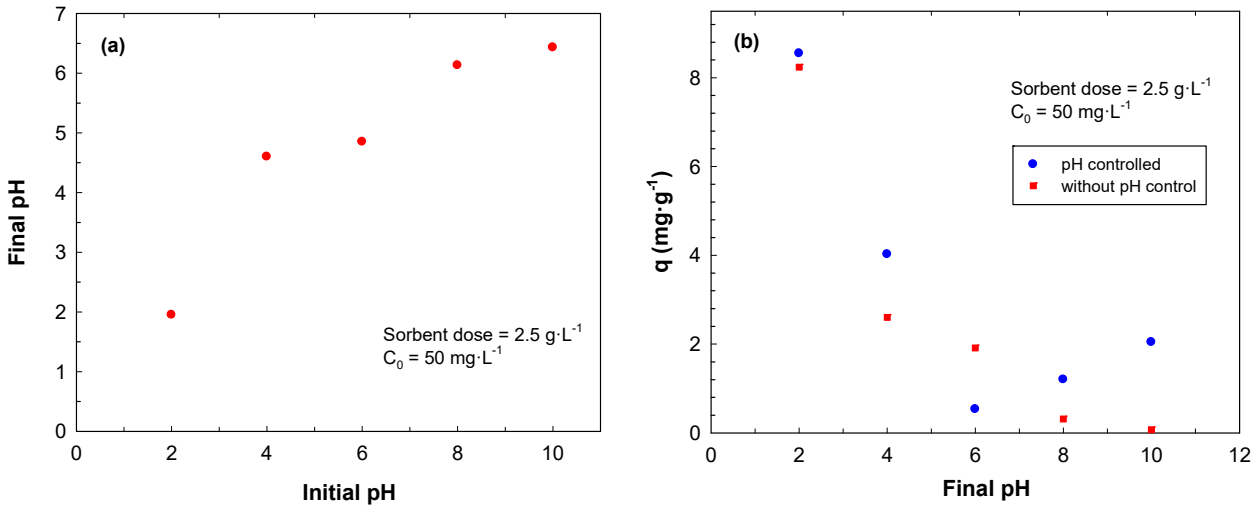

Figure 5. Effect of pH on adsorption capacity of Orange II on *Aloe vera*: (**a**) final pH versus initial pH in assays without pH control, (**b**) equilibrium O-II uptake as a function of final pH in assays with and without pH control.

Figure 5b shows the equilibrium adsorption capacity of Orange II versus the final pH of the solution in the tests carried out with and without pH control. In these experiments, the highest adsorption capacity of O-II was obtained at pH 2 (8.55 mg·g^{-1}). This behavior was to be expected in light of the point of zero charge value of AV (4.1 to 4.5) and the anionic nature of the dye. When the pH is lower than the pH_{zpc}, the AV surface is positively charged due to protonation of the surface hydroxyl groups. These positively charged groups (AV-OH_2^+) increase as the pH decreases. At pH values greater than the pH_{zpc}, the AV surface is deprotonated and becomes negatively charged, with the negatively charged surface groups (AV-O^-) increasing as pH increases. As for the dye, Orange II (pKa 10.6 and 1) [74] in aqueous solutions can be present in three different chemical forms depending on the pH of the solution: doubly protonated (H_2-O-II), prevailing for pH values less than 1, mono-protonated (H-O-II$^-$) after deprotonation of the sulfonate group, form dominant for pH values between 1 and 10.6, and non-protonated (O-II^{2-}) after deprotonation of the sulfonate and OH of the naphthalene groups, which is the predominant form for pH values greater than 10.6. At pH levels < pH_{zpc}, the sulfonate group in O-II is deprotonated and practically only the mono-protonated form of the dye (H-O-II$^-$) is present in the solution. Therefore,

as pH decreases, the adsorption capacity of the adsorbent increases due to the increase in positive charge of the AV surface and thus of the electrostatic attraction between the positively charged surface groups (AV-OH_2^+) and the negatively charged dye (H-O-II^-). In addition to this electrostatic attraction, adsorption is also due to other interactions between the dye and the AV surface, such as: van der Waals interactions (polar nature of O-II), π–π interactions (between aromatic rings), and hydrogen bond formation (high electronegativity of O, N and S in O-II). On the other hand, at pH levels > pH_{zpc}, the adsorption capacity of AV is significantly reduced because the adsorbent surface is deprotonated and therefore negatively charged (AV-O^-), like the dye (H-O-II^-). Consequently, there is no electrostatic attraction, and only van der Waals forces and π–π interactions contribute to O-II adsorption.

Similar results have been obtained by other authors, and they can be explained by a change in the concentration of protons, as discussed above. O-II is an anionic dye; at low pH values, some of the functional groups present in the biosorbent are protonated and its surface is positively charged, favoring the adsorption of the anionic dye [61,73,75].

3.4. Biosorption Kinetics

Determination of the optimum contact time is very important for the consideration of biosorption as a suitable treatment for wastewater treatment [42,49,52]. Therefore, the kinetics of O-II biosorption on *Aloe vera* were studied via measuring the amounts of dye adsorbed at different time intervals (Figure 6).

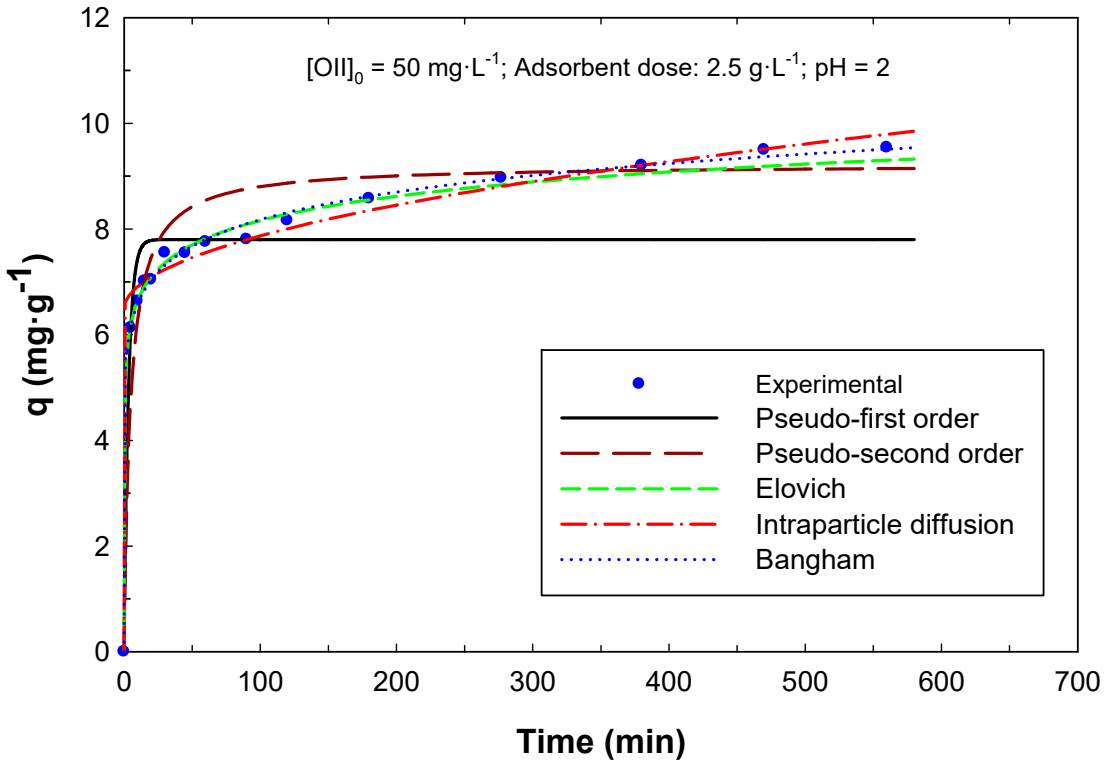

Figure 6. Orange II biosorption kinetics on *Aloe vera*. Experimental data and data fit to the kinetic models used.

At the beginning of the test, the adsorption rate was fast, since in the adsorbent solid there are more active places available, and it was far from equilibrium. Additionally, the difference between the concentrations of O-II in the solution and on the surface of the adsorbent material was very high. Most of the O-II adsorption took place within the first 5–10 min, and as the time increased, the adsorption rate decreased until equilibrium was reached and there were no longer any free active sites in the biosorbent to be occupied by the adsorbate. Equilibrium was reached at a contact time of approximately 6 h.

The adsorption rate for removing dyes from aqueous solutions depends on operation conditions and the characteristics of the adsorbate and biosorbent [42,64]. The data obtained were fitted to different kinetic models to evaluate the mechanisms controlling dye adsorption. Five kinetic models were used in this research: pseudo—first order, pseudo—second order, Elovich, intraparticle diffusion, and Bangham [52,56,76].

The experimental data were fitted to the kinetic models using nonlinear regression analysis, minimizing the average relative error function (ARE). This value was also used to evaluate the validity of the model. The models' characteristic parameters are given in Table 6 and the curves corresponding to the adsorption rate data calculated with the different models used are shown in Figure 6.

Table 6. Kinetic parameters obtained for the adsorption of O-II by *Aloe vera*.

Kinetic Model	Parameters	
Pseudo—first order	q_e ($mg \cdot g^{-1}$)	7.8
	k_1 (min^{-1})	0.308
	ARE (%)	7.87
Pseudo—second order	q_e ($mg \cdot g^{-1}$)	9.22
	k_2 ($g \cdot mg^{-1} \cdot min^{-1}$)	0.0229
	h ($mg \cdot g^{-1} \cdot min^{-1}$)	1.95
	ARE (%)	6.43
Elovich	α ($mg \cdot g^{-1} \cdot min^{-1}$)	1449
	β ($g \cdot mg^{-1}$)	1.506
	ARE (%)	1.46
Intraparticle diffusion	k_d ($mg \cdot g^{-1} \cdot min^{-0.5}$)	0.1406
	C ($mg \cdot g^{-1}$)	6.46
	ARE (%)	2.23
Bangham	k_B ($L \cdot g^{-1}$)	0.122
	σ	0.119
	ARE (%)	1.063

The kinetic model that best fits the experimental data is the Bangham model, with an average relative error value of 1.06%. The Elovich (ARE = 1.45%) and intraparticle diffusion (ARE = 2.22%) models also fit the experimental data quite well. Both the Bangham model and the intraparticle diffusion model (using the Weber and Morris equation) are internal diffusional models. Therefore, the slowest stage could be the mass transfer to the interior of the particle [56]. On the other hand, Elovich's model is an adsorption model in which adsorption is considered the slowest step and it is normally applied when chemisorption takes place [56].

The ARE values for the pseudo first order and pseudo second order equations are greater than 6%, therefore, in this case, they were not considered applicable to describe the biosorption kinetics of O-II on *Aloe vera*.

3.5. Adsorption Isotherm

Adsorption isotherm relates the concentrations of adsorbate in the solution and in the adsorbent solid at equilibrium, and its study allows the estimation of the amount of adsorbent needed and the characteristics of the equipment in the adsorption. The application of different isotherm models is useful to provide information about the possible mechanisms that take places during adsorption [42,52].

Figure 7 shows the experimental equilibrium data obtained at pH = 2 (adsorption capacity O-II at equilibrium, q_e, versus the concentration of O-II in the solution, C_e).

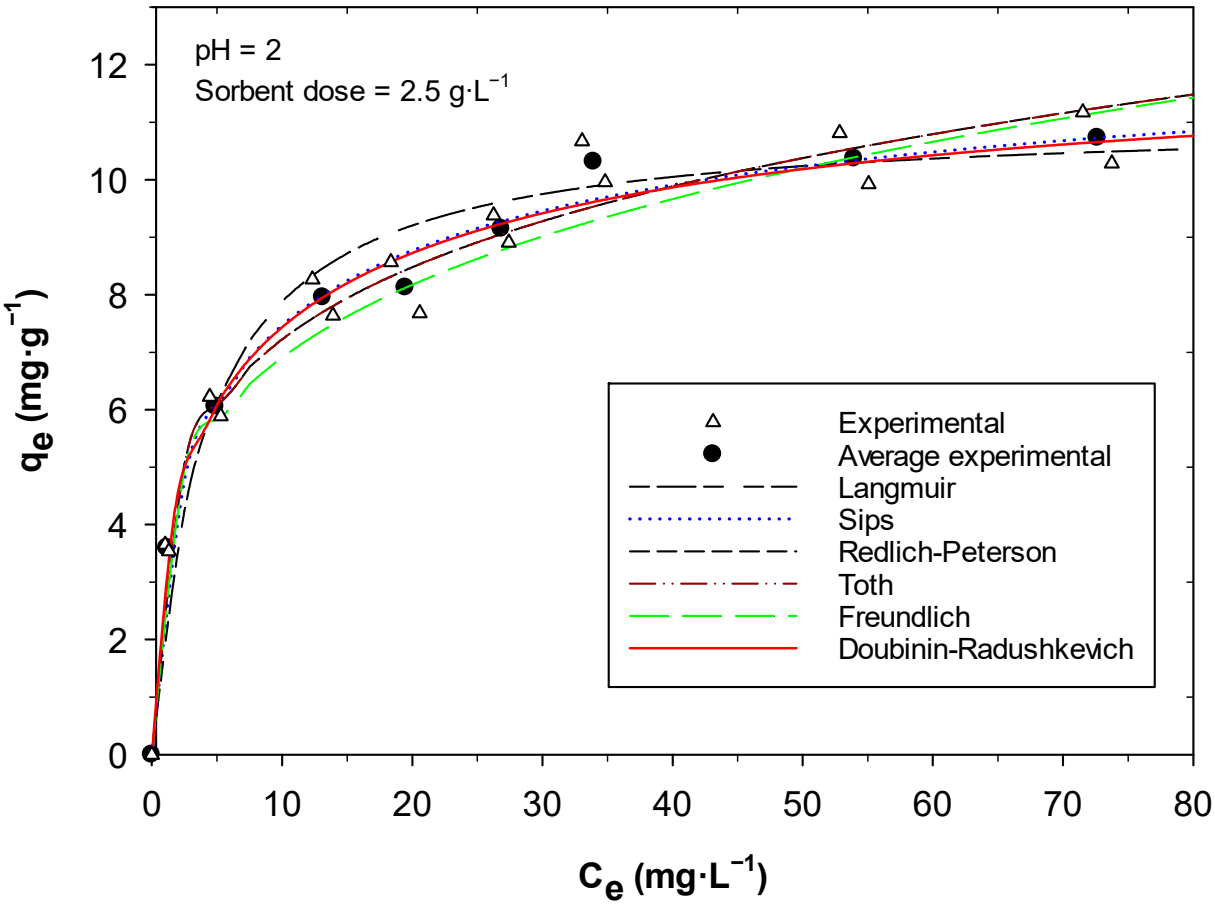

Figure 7. Equilibrium isotherm for Orange II biosorption on *Aloe vera*. Experimental values and values fit to different isotherm models.

The adsorption capacity increased as the concentration of O-II in the solution increased until the adsorbate reached its saturation value. The shape of the curve (concave down, Langmuir type, L2, in Giles classification) indicates that adsorption was favorable [42,52].

At low-equilibrium solution concentrations, the slope of the curve is high, since there are numerous free active sites in the adsorbent that can be easily occupied by the adsorbate. On the other hand, when the concentration of the solution increases, the slope of the curve decreases, which indicates that adsorption takes place in less accessible active sites and that the adsorption capacity tends to stabilize when it approaches equilibrium. Finally, at sufficiently high concentrations, saturation occurs, and the maximum O-II adsorption capacity is reached.

The data obtained were analyzed with different isotherm models: Langmuir, Freundlich, Dubinin–Radushkevich, Redlich–Peterson, Sips, and Toth. The values calculated by the models can be seen in Figure 7.

Table 7 collects the characteristic model parameters and the values of ARE obtained when adjusting the experimental data with non-linear regression to the different models mentioned above.

The ARE value for the Toth isotherm model was lowest compared with the other isotherm models used. Although, it is also observed that models such as the Dubinin–Radushkevich and Sips fit well, with an average relative error of 1.83% and 2.11%, respectively, and the Redlich–Peterson model presented an ARE of 3.62%. The Langmuir and Freundlich models exceed the value of 4.9% relative error.

Table 7. Model isotherm parameters and ARE values for O-II biosorption on *Aloe vera*.

Isotherm Model	Parameters	
Langmuir	q_{mL} (mg·g^{-1})	11.064
	K_L (L·mg^{-1})	0.248
	ARE (%)	6.99
Freundlich	K_F ((mg·g^{-1})·(mg·L^{-1}) $^{-1/n}$)	3.961
	n	4.13
	ARE (%)	4.86
Redlich–Peterson	K_R (L·g^{-1})	20.26
	α_R (L·mg^{-1})$^{\beta}$	4.37
	β	0.79
	ARE (%)	3.62
Sips	q_{mS} (mg·g^{-1})	13.29
	K_s (L$^{1/nS}$·mmol$^{-1/nS}$)	0.326
	n_s	1.68
	ARE (%)	2.11
Toth	q_{mT} (mg·g^{-1})	15.87
	K_T (L·mg^{-1})^{T}$_T$	1.903
	T_T	2.67
	ARE (%)	1.67
Dubinin–Radushkevich	q_{mDR} (mmol·g^{-1})	0.0341
	K_{DR} (mol^2·kJ^{-2})	0.0060
	E (kJ·mol^{-1})	9.118
	ARE (%)	1.83

The Langmuir, Sips, Toth, and Dubinin–Radushkevich models contain the maximum adsorption capacity as a parameter, so its value was determined by fitting the experimental data to these models. The values obtained are between 11.1 and 15.9 mg·g^{-1} and are consistent with the experimental data.

The Toth isotherm gives a better result than the Langmuir isotherm, as was expected, since it is a variation of the Langmuir model. The Toth equation is a modified empirical form used to describe heterogeneous adsorption systems at low and high adsorbate concentrations. The value of n_T = 2.67 indicates the heterogeneity of the adsorption [77,78].

The parameter n of the Freundlich isotherm is between 0 and 10, indicating that adsorption is favorable, which is also confirmed by the value of the parameter β = 0.79 of the Redlich–Peterson isotherm (which should be between 0 and 2) and the equilibrium R_L parameter obtained from the Langmuir isotherm (which should be between 0 and 1). Figure 8 shows the values of R_L together with the parameter θ (representing the fraction of sorption sites occupied by the adsorbate at equilibrium), versus the initial concentration (C_0). As can be seen, the values of R_L and θ fall within the range that indicates that the adsorption of Orange II on *Aloe vera* is favorable [52,58].

The mean free energy of adsorption (E) calculated from the Dubinin–Radushkevich isotherm was 9.118 kJ·mol^{-1}, suggesting ion exchange adsorption [52,59].

Finally, to compare the efficiency of the adsorbent used in this study for O-II removal, Table 8 shows the values of the maximum adsorption capacity of other adsorbent materials found in the literature.

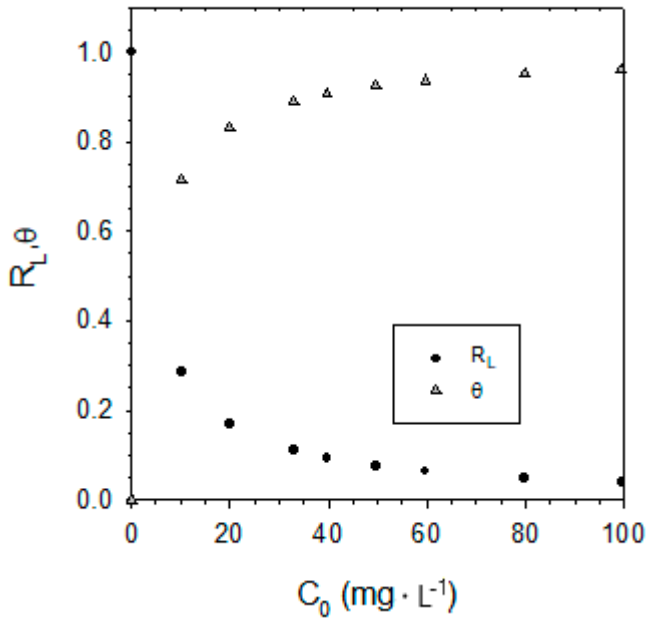

Figure 8. Equilibrium parameter (R_L) and surface coverage (θ) versus initial O-II concentration.

Table 8. Maximum adsorption capacities of several adsorbents found in the literature.

Adsorbent	q_m (mg·g^{-1})	Reference
Surfactant-modified zeolite	3.62	[79]
Olive stone by-product	13.2	[80]
Aloe vera	15.87	This study
Canola stalks	25.6	[81]
Spent brewery grains	30.5	[82]
Magnetic graphene/chitosan	42.7	[83]

3.6. Adsorption Mechanisms

Considering the heterogeneous nature of the adsorbent solid, as well as the chemical structure of the O-II dye molecule, which possesses several aromatics rings as well as ionizable functional groups, it can be indicated that the mechanisms involved in adsorption are complex. However, several possible mechanisms can be suggested: electrostatic attraction, π–π interactions, and hydrogen bonding.

Electrostatic interactions may exist between functional groups on the AV surface and the dye molecules. In this sense, the pH of the solution can influence the existing electrostatic interactions in the adsorption of O-II by AV. As previously indicated, the pH_{zpc} is 4.1–4.5, so that under the selected operating conditions (pH = 2), the pH < pH_{zpc}, and the surface of the adsorbent solid is therefore positively charged. At this pH, the O-II molecule is negatively charged, being in its ionized form H-O-II^-. In this way, electrostatic interactions are established between the positively charged solid surface and the negatively charged adsorbate molecules.

In accordance with the FTIR spectrum of the adsorbent solid, it can be indicated that -OH groups, C-H groups in aromatic rings, C=C bonds of the aromatic rings, and phenolic C-O bonds can take part in the adsorption of O-II by AV. The presence of aromatic rings and phenolic groups suggests that π–π interactions may occur during the adsorption process. This π–π interaction may be one of the mechanisms implicated when the adsorbate is an organic substance with aromatic rings. This interaction takes place between electron-poor and electron-rich structures [84]. The O-II molecule possesses aromatic π-systems that can act as electron acceptors, particularly due to the high electronegativity of the O, N, and S

atoms present in its chemical structure. O, N, and S atoms bonded to aromatic rings have a high electron-holding capacity, making the aromatic ring electron-deficient and acting as a π-acceptor. The C=C bonding of the aromatic ring and the hydroxyl groups on the AV surface make them electron donors [85,86].

On the other hand, hydrogen bonding interactions can also occur in the adsorption process. The adsorbent surface contains several functional groups, such as C-OH and COOH, and aromatic rings that can interact with the aromatic rings and the nitrogen and oxygen atoms of the O-II molecules through H-bonds. Under acidic conditions, free H+ in the medium can also contribute to the formation of hydrogen bonds between the adsorbent surface and the O-II molecules.

Figure 9 shows the different interactions between the adsorbent and the dye molecule schematically.

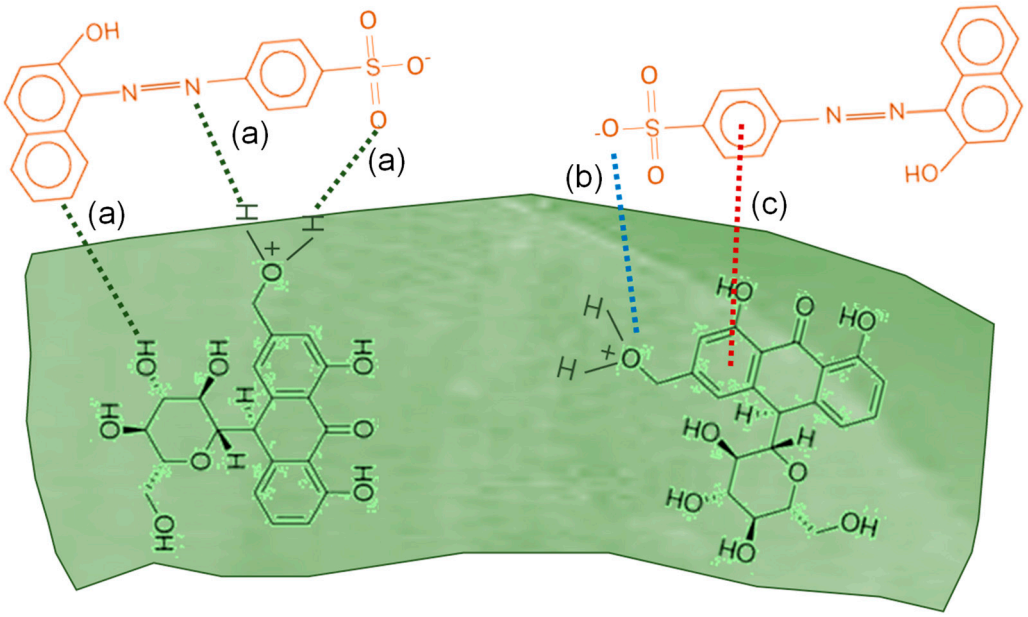

Figure 9. Diagram of the proposed adsorption mechanism: (**a**) H-bond interaction, (**b**) electrostatic interaction, and (**c**) π–π interaction.

4. Conclusions

Aloe vera can be satisfactorily used as an adsorbent material for the removal of Orange II dye from aqueous solutions.

The Box–Behnken experiment design, using three parameters (adsorbent dose, initial dye concentration, and contact time), has given satisfactory results for the optimization of the adsorption process. The coefficient of the determination (R^2) value obtained (0.9993) shows that the model adequately represents the relationship between each response and the chosen variables.

The pH influences the adsorption capacity, obtaining the highest adsorption capacity of O-II (8.55 $mg \cdot g^{-1}$) at pH 2. The levels of O-II biosorption decreased sharply when the pH levels of the dye solution increased.

At 25 °C, equilibrium was reached at a contact time of approximately 6 h.

From the kinetic models studied, the one that best describes the adsorption of Orange II on *Aloe vera* is the Bangham model (ARE = 1.06%).

The isotherm model that best represents the experimental data is the Toth model. The maximum adsorption capacity obtained by this model was 15.87 $mg \cdot g^{-1}$.

The adsorption of Orange II on *Aloe vera* is favorable because with this method, the equilibrium parameter R_L is between 0 and 1; the constant n of the Freundlich isotherm is between 0 and 10; and the value of the constant β, of the Redlich–Peterson isotherm, is between 0 and 2.

Author Contributions: Conceptualization, M.I.A., M.L., J.F.O., V.F.M. and A.B.P.-M.; methodology, M.I.A., M.L., J.F.O., V.F.M., A.B.P.-M. and A.C.; software, M.I.A., M.L., J.F.O., V.F.M. and A.B.P.-M.; validation, M.I.A., M.L., J.F.O., V.F.M. and A.B.P.-M.; formal analysis, M.I.A., M.L., J.F.O., V.F.M., A.B.P.-M. and A.C.; investigation, M.I.A., M.L., J.F.O., V.F.M., A.B.P.-M. and A.C.; resources, M.I.A., M.L., J.F.O., V.F.M. and A.B.P.-M.; data curation, M.I.A., M.L., J.F.O., V.F.M. and A.B.P.-M.; writing—original draft preparation, M.I.A., M.L., J.F.O., V.F.M. and A.B.P.-M.; writing—review and editing, M.I.A., M.L., J.F.O., V.F.M. and A.B.P.-M. All authors have read and agreed to the published version of the manuscript.

Funding: This research received no external funding.

Data Availability Statement: The data presented in this study are available on request from the corresponding author.

Conflicts of Interest: The authors declare no conflict of interest.

References

1. Bazin, I.; Ibn Hadj Hassine, A.; Haj Hamouda, Y.; Mnif, W.; Bartegi, A.; Lopez-Ferber, M.; De Waard, M.; Gonzalez, C. Estrogenic and Anti-Estrogenic Activity of 23 Commercial Textile Dyes. *Ecotoxicol. Environ. Saf.* **2012**, *85*, 131–136. [CrossRef] [PubMed]
2. Birhanli, A.; Ozmen, M. Evaluation of the Toxicity and Teratogenity of Six Commercial Textile Dyes Using the Frog Embryo Teratogenesis Assay-Xenopus. *Drug Chem. Toxicol.* **2005**, *28*, 51–65. [CrossRef] [PubMed]
3. Oliveira, D.P.; Carneiro, P.A.; Sakagami, M.K.; Zanoni, M.V.B.; Umbuzeiro, G.A. Chemical Characterization of a Dye Processing Plant Effluent-Identification of the Mutagenic Components. *Mutat. Res. Genet. Toxicol. Environ. Mutagen.* **2007**, *626*, 135–142. [CrossRef]
4. Mustereţ, C.P.; Teodosiu, C. Removal of Persistent Organic Pollutants from Textile Wastewater by Membrane Processes. *Environ. Eng. Manag. J.* **2007**, *6*, 175–187. [CrossRef]
5. Karcher, S.; Kornmüller, A.; Jekel, M. Anion Exchange Resins for Removal of Reactive Dyes from Textile Wastewaters. *Water Res.* **2002**, *36*, 4717–4724. [CrossRef] [PubMed]
6. Vieira, A.P.; Santana, S.A.A.; Bezerra, C.W.B.; Silva, H.A.S.; Chaves, J.A.P.; de Melo, J.C.P.; da Silva Filho, E.C.; Airoldi, C. Kinetics and Thermodynamics of Textile Dye Adsorption from Aqueous Solutions Using Babassu Coconut Mesocarp. *J. Hazard. Mater.* **2009**, *166*, 1272–1278. [CrossRef] [PubMed]
7. Ogugbue, C.J.; Sawidis, T. Bioremediation and Detoxification of Synthetic Wastewater Containing Triarylmethane Dyes by Aeromonas Hydrophila Isolated from Industrial Effluent. *Biotechnol. Res. Int.* **2011**, *2011*, 967925. [CrossRef]
8. Petcu, A.R.; Lazar, C.A.; Rogozea, E.A.; Olteanu, N.L.; Meghea, A.; Mihaly, M. Nonionic Microemulsion Systems Applied for Removal of Ionic Dyes Mixtures from Textile Industry Wastewaters. *Sep. Purif. Technol.* **2016**, *158*, 155–159. [CrossRef]
9. Wang, J.; Yao, J.; Wang, L.; Xue, Q.; Hu, Z.; Pan, B. Multivariate Optimization of the Pulse Electrochemical Oxidation for Treating Recalcitrant Dye Wastewater. *Sep. Purif. Technol.* **2020**, *230*, 115851. [CrossRef]
10. Liu, J.; Liu, A.; Wang, W.; Li, R.; Zhang, W. xian Feasibility of Nanoscale Zero-Valent Iron (NZVI) for Enhanced Biological Treatment of Organic Dyes. *Chemosphere* **2019**, *237*, 124470. [CrossRef]
11. Huang, Z.; Wang, T.; Shen, M.; Huang, Z.; Chong, Y.; Cui, L. Coagulation Treatment of Swine Wastewater by the Method of In-Situ Forming Layered Double Hydroxides and Sludge Recycling for Preparation of Biochar Composite Catalyst. *Chem. Eng. J.* **2019**, *369*, 784–792. [CrossRef]
12. Visa, M.; Carcel, R.A.; Andronic, L.; Duta, A. Advanced Treatment of Wastewater with Methyl Orange and Heavy Metals on TiO_2, Fly Ash and Their Mixtures. *Catal. Today* **2009**, *144*, 137–142. [CrossRef]
13. Rondina, D.J.G.; Ymbong, D.V.; Cadutdut, M.J.M.; Nalasa, J.R.S.; Paradero, J.B.; Mabayo, V.I.F.; Arazo, R.O. Utilization of a Novel Activated Carbon Adsorbent from Press Mud of Sugarcane Industry for the Optimized Removal of Methyl Orange Dye in Aqueous Solution. *Appl. Water Sci.* **2019**, *9*, 181. [CrossRef]
14. Zhao, P.; Zhang, R.; Wang, J. Adsorption of Methyl Orange from Aqueous Solution Using Chitosan/Diatomite Composite. *Water Sci. Technol.* **2017**, *75*, 1633–1642. [CrossRef] [PubMed]
15. Chaukura, N.; Murimba, E.C.; Gwenzi, W. Synthesis, Characterisation and Methyl Orange Adsorption Capacity of Ferric Oxide–Biochar Nano-Composites Derived from Pulp and Paper Sludge. *Appl. Water Sci.* **2017**, *7*, 2175–2186. [CrossRef]
16. Krika, F.; Benlahbib, O.e.F. Removal of Methyl Orange from Aqueous Solution via Adsorption on Cork as a Natural and Low-Coast Adsorbent: Equilibrium, Kinetic and Thermodynamic Study of Removal Process. *Desalination Water Treat.* **2015**, *53*, 3711–3723. [CrossRef]
17. Rafatullah, M.; Sulaiman, O.; Hashim, R.; Ahmad, A. Adsorption of Methylene Blue on Low-Cost Adsorbents: A Review. *J. Hazard. Mater.* **2010**, *177*, 70–80. [CrossRef]
18. Aguayo-Villarreal, I.A.; Ramírez-Montoya, L.A.; Hernández-Montoya, V.; Bonilla-Petriciolet, A.; Montes-Morán, M.A.; Ramírez-López, E.M. Sorption Mechanism of Anionic Dyes on Pecan Nut Shells (*Carya illinoinensis*) Using Batch and Continuous Systems. *Ind. Crops Prod.* **2013**, *48*, 89–97. [CrossRef]

19. Arshadi, M.; Salimivahid, F.; Salvacion, J.W.L.; Soleymanzadeh, M. Adsorption Studies of Methyl Orange on an Immobilized Mn-Nanoparticle: Kinetic and Thermodynamic. *RSC Adv.* **2014**, *4*, 16005–16017. [CrossRef]
20. Oloo, C.M.; Onyari, J.M.; Wanyonyi, W.C.; Wabomba, J.N.; Muinde, V.M. Adsorptive Removal of Hazardous Crystal Violet Dye Form Aqueous Solution Using Rhizophora Mucronata Stem-Barks: Equilibrium and Kinetics Studies. *Environ. Chem. Ecotoxicol.* **2020**, *2*, 64–72. [CrossRef]
21. Crini, G.; Badot, P.-M. Application of Chitosan, a Natural Aminopolysaccharide, for Dye Removal from Aqueous Solutions by Adsorption Processes Using Batch Studies: A Review of Recent Literature. *Prog. Polym. Sci.* **2008**, *33*, 399–447. [CrossRef]
22. Haitham, K.; Razak, S.; Nawi, M.A. Kinetics and Isotherm Studies of Methyl Orange Adsorption by a Highly Recyclable Immobilized Polyaniline on a Glass Plate. *Arab. J. Chem.* **2019**, *12*, 1595–1606. [CrossRef]
23. Vučurović, V.M.; Razmovski, R.N.; Miljić, U.D.; Puškaš, V.S. Removal of Cationic and Anionic Azo Dyes from Aqueous Solutions by Adsorption on Maize Stem Tissue. *J. Taiwan Inst. Chem. Eng.* **2014**, *45*, 1700–1708. [CrossRef]
24. Salih, S.J.; Abdul Kareem, A.S.; Anwer, S.S. Adsorption of Anionic Dyes from Textile Wastewater Utilizing Raw Corncob. *Heliyon* **2022**, *8*, e10092. [CrossRef] [PubMed]
25. Yagub, M.T.; Sen, T.K.; Afroze, S.; Ang, H.M. Dye and Its Removal from Aqueous Solution by Adsorption: A Review. *Adv. Colloid Interface Sci.* **2014**, *209*, 172–184. [CrossRef] [PubMed]
26. Haque, A.N.M.A.; Sultana, N.; Sayem, A.S.M.; Smriti, S.A. Sustainable Adsorbents from Plant-Derived Agricultural Wastes for Anionic Dye Removal: A Review. *Sustainability* **2022**, *14*, 11098. [CrossRef]
27. Bhomick, P.C.; Supong, A.; Kumar, S.; Sema, A.I.; Merry, T.; Sinha, D. Utilization of Pinus Kesiya and Schima Wallichii Biomass-Derived Activated Carbon for Methylene Blue Removal: Adsorption Performance and Mechanistic Insights. *Water Conserv. Sci. Eng.* **2023**, *8*, 48. [CrossRef]
28. Li, L.; Li, X.; Yan, C.; Guo, W.; Yang, T.; Fu, J.; Tang, J.; Hu, C. Optimization of Methyl Orange Removal from Aqueous Solution by Response Surface Methodology Using Spent Tea Leaves as Adsorbent. *Front. Environ. Sci. Eng.* **2014**, *8*, 496–502. [CrossRef]
29. Bazrafshan, E.; Zarei, A.A.; Nadi, H.; Zazouli, M.A. Adsorptive Removal of Methyl Orange and Reactive Red 198 Dyes by Moringa Peregrina Ash. *Indian J. Chem. Technol.* **2014**, *21*, 105–113.
30. Ahmaruzzaman, M. Removal of Methyl Orange from Aqueous Solution Using Activated Papaya Leaf. *Sep. Sci. Technol.* **2012**, *47*, 2381–2390.
31. Fadhil, O.H.; Eisa, M.Y. Removal of Methyl Orange from Aqueous Solutions by Adsorption Using Corn Leaves as Adsorbent Material. *J. Eng.* **2019**, *25*, 55–69. [CrossRef]
32. Jawad, A.H.; Ngoh, Y.S.; Radzun, K.A. Utilization of Watermelon (*Citrullus lanatus*) Rinds as a Natural Low-Cost Biosorbent for Adsorption of Methylene Blue: Kinetic, Equilibrium and Thermodynamic Studies. *J. Taibah Univ. Sci.* **2018**, *12*, 371–381. [CrossRef]
33. Jawad, A.H.; Mamat, N.F.H.; Abdullah, M.F.; Ismail, K. Adsorption of Methylene Blue onto Acid-Treated Mango Peels: Kinetic, Equilibrium and Thermodynamic Study. *Desalination Water Treat.* **2017**, *59*, 210–219. [CrossRef]
34. Jawad, A.H.; Waheeb, A.S.; Rashid, R.A.; Nawawi, W.I.; Yousif, E. Equilibrium Isotherms, Kinetics, and Thermodynamics Studies of Methylene Blue Adsorption on Pomegranate (*Punica granatum*) Peels as a Natural Low-Cost Biosorbent. *Desalination Water Treat.* **2018**, *105*, 322–331. [CrossRef]
35. Amel, K.; Hassen, M.A.; Kerroum, D. Isotherm and Kinetics Study of Biosorption of Cationic Dye onto Banana Peel. *Energy Procedia* **2012**, *19*, 286–295. [CrossRef]
36. Jawad, A.H.; Kadhum, A.M.; Ngoh, Y.S. Applicability of Dragon Fruit (*Hylocereus polyrhizus*) Peels as Low-Cost Biosorbent for Adsorption of Methylene Blue from Aqueous Solution: Kinetics, Equilibrium and Thermodynamics Studies. *Desalination Water Treat.* **2018**, *109*, 231–240. [CrossRef]
37. Bulgariu, L.; Escudero, L.B.; Bello, O.S.; Iqbal, M.; Nisar, J.; Adegoke, K.A.; Alakhras, F.; Kornaros, M.; Anastopoulos, I. The Utilization of Leaf-Based Adsorbents for Dyes Removal: A Review. *J. Mol. Liq.* **2019**, *276*, 728–747. [CrossRef]
38. Baruah, A.; Bordoloi, M.; Deka Baruah, H.P. Aloe vera: A Multipurpose Industrial Crop. *Ind. Crops Prod.* **2016**, *94*, 951–963. [CrossRef]
39. Kumar, V.; Yadav, S.K. Plant-Mediated Synthesis of Silver and Gold Nanoparticles and Their Applications. *J. Chem. Technol. Biotechnol.* **2009**, *84*, 151–157. [CrossRef]
40. Soltanizadeh, N.; Ghiasi-Esfahani, H. Qualitative Improvement of Low Meat Beef Burger Using *Aloe vera*. *Meat Sci.* **2014**, *99*, 75–80. [CrossRef]
41. Alğin Yapar, E. Herbal Cosmetics and Novel Drug Delivery Systems. *Indian J. Pharm. Educ. Res.* **2017**, *51*, S152–S158. [CrossRef]
42. Hanafiah, M.A.K.M.; Mohd Jamaludin, S.Z.; Khalid, K.; Ibrahim, S. Methylene Blue Adsorption on *Aloe vera* Rind Powder: Kinetics, Isotherm and Mechanisms. *Nat. Environ. Pollut. Technol.* **2018**, *17*, 1055–1064.
43. Noli, F.; Kapashi, E.; Kapnisti, M. Biosorption of Uranium and Cadmium Using Sorbents Based on *Aloe vera* Wastes. *J. Environ. Chem. Eng.* **2019**, *7*, 102985. [CrossRef]
44. Giannakoudakis, D.A.; Hosseini-Bandegharaei, A.; Tsafrakidou, P.; Triantafyllidis, K.S.; Kornaros, M.; Anastopoulos, I. *Aloe vera* Waste Biomass-Based Adsorbents for the Removal of Aquatic Pollutants: A Review. *J. Environ. Manag.* **2018**, *227*, 354–364. [CrossRef]
45. El-Azazy, M.; Dimassi, S.; El-Shafie, A.; Issa, A. Bio-Waste *Aloe vera* Leaves as an Efficient Adsorbent for Titan Yellow from Wastewater: Structuring of a Novel Adsorbent Using Plackett-Burman Factorial Design. *Appl. Sci.* **2019**, *9*, 4856. [CrossRef]

46. Sharif, K.M.; Rahman, M.M.; Azmir, J.; Mohamed, A.; Jahurul, M.H.A.; Sahena, F.; Zaidul, I.S.M. Experimental Design of Supercritical Fluid Extraction—A Review. *J. Food Eng.* **2014**, *124*, 105–116. [CrossRef]
47. Tripathi, P.; Srivastava, V.C.; Kumar, A. Optimization of an Azo Dye Batch Adsorption Parameters Using Box-Behnken Design. *Desalination* **2009**, *249*, 1273–1279. [CrossRef]
48. Montgomery, D.C. *Design and Analysis of Experiments*, 8th ed.; John Wiley & Sons, Inc.: Hoboken, NJ, USA, 2012; ISBN 978-1-118-09793-9.
49. Liu, X.; Han, B.; Su, C.-L.; Han, Q.; Chen, K.-J.; Chen, Z.-Q. Optimization and Mechanisms of Biosorption Process of Zn(II) on Rape Straw Powders in Aqueous Solution. *Environ. Sci. Pollut. Res.* **2019**, *26*, 32151–32164. [CrossRef]
50. Ravikumar, K.; Krishnan, S.; Ramalingam, S.; Balu, K. Optimization of Process Variables by the Application of Response Surface Methodology for Dye Removal Using a Novel Adsorbent. *Dye. Pigment.* **2007**, *72*, 66–74. [CrossRef]
51. Katubi, K.M.; Amari, A.; Harharah, H.N.; Eldirderi, M.M.; Tahoon, M.A.; Rebah, F. Ben *Aloe vera* as Promising Material for Water Treatment: A Review. *Processes* **2021**, *9*, 782. [CrossRef]
52. Meseguer, V.F.; Ortuño, J.F.; Aguilar, M.I.; Pinzón-Bedoya, M.L.; Lloréns, M.; Sáez, J.; Pérez-Marín, A.B. Biosorption of Cadmium (II) from Aqueous Solutions by Natural and Modified Non-Living Leaves of Posidonia Oceanica. *Environ. Sci. Pollut. Res.* **2016**, *23*, 24032–24046. [CrossRef] [PubMed]
53. Fiol, N.; Villaescusa, I. Determination of Sorbent Point Zero Charge: Usefulness in Sorption Studies. *Environ. Chem. Lett.* **2009**, *7*, 79–84. [CrossRef]
54. Wang, Y.X.; Ngo, H.H.; Guo, W.S. Preparation of a Specific Bamboo Based Activated Carbon and Its Application for Ciprofloxacin Removal. *Sci. Total Environ.* **2015**, *533*, 32–39. [CrossRef] [PubMed]
55. Bouchelkia, N.; Tahraoui, H.; Amrane, A.; Belkacemi, H.; Bollinger, J.C.; Bouzaza, A.; Zoukel, A.; Zhang, J.; Mouni, L. Jujube Stones Based Highly Efficient Activated Carbon for Methylene Blue Adsorption: Kinetics and Isotherms Modeling, Thermodynamics and Mechanism Study, Optimization via Response Surface Methodology and Machine Learning Approaches. *Process Saf. Environ. Prot.* **2023**, *170*, 513–535. [CrossRef]
56. Largitte, L.; Pasquier, R. A Review of the Kinetics Adsorption Models and Their Application to the Adsorption of Lead by an Activated Carbon. *Chem. Eng. Res. Des.* **2016**, *109*, 495–504. [CrossRef]
57. Ighalo, J.O.; Adeniyi, A.G. Adsorption of Pollutants by Plant Bark Derived Adsorbents: An Empirical Review. *J. Water Process Eng.* **2020**, *35*, 101228. [CrossRef]
58. Majd, M.M.; Kordzadeh-Kermani, V.; Ghalandari, V.; Askari, A.; Sillanpää, M. Adsorption Isotherm Models: A Comprehensive and Systematic Review (2010−2020). *Sci. Total Environ.* **2022**, *812*, 151334. [CrossRef]
59. Hu, Q.; Zhang, Z. Application of Dubinin–Radushkevich Isotherm Model at the Solid/Solution Interface: A Theoretical Analysis. *J. Mol. Liq.* **2019**, *277*, 646–648. [CrossRef]
60. Reddy, A.V.B.; Rafiq, R.; Ahmad, A.; Maulud, A.S.; Moniruzzaman, M. Cross-Linked Ionic Liquid Polymer for the Effective Removal of Ionic Dyes from Aqueous Systems: Investigation of Kinetics and Adsorption Isotherms. *Molecules* **2022**, *27*, 7775. [CrossRef]
61. Wu, Y.; Hu, Y.; Xie, Z.; Feng, S.; Li, B.; Mi, X. Characterization of Biosorption Process of Acid Orange 7 on Waste Brewery's Yeast. *Appl. Biochem. Biotechnol.* **2011**, *163*, 882–894. [CrossRef]
62. Ray, A.; Ghosh, S. Chemometrics for Functional Group Distribution, and UV Absorption Potential of *Aloe vera* L. Gel at Different Growth Periods. *Mater. Today Proc.* **2018**, *5*, 22245–22253. [CrossRef]
63. Jamoussi, B.; Chakroun, R.; Jablaoui, C.; Rhazi, L. Efficiency of Acacia Gummifera Powder as Biosorbent for Simultaneous Decontamination of Water Polluted with Metals. *Arab. J. Chem.* **2020**, *13*, 7459–7481. [CrossRef]
64. Kousha, M.; Daneshvar, E.; Dopeikar, H.; Taghavi, D.; Bhatnagar, A. Box-Behnken Design Optimization of Acid Black 1 Dye Biosorption by Different Brown Macroalgae. *Chem. Eng. J.* **2012**, *179*, 158–168. [CrossRef]
65. Lin, Z.; Hu, Y.; Yuan, Y.; Hu, B.; Wang, B. Comparative Analysis of Kinetics and Mechanisms for Pb(II) Sorption onto Three Kinds of Microplastics. *Ecotoxicol. Environ. Saf.* **2021**, *208*, 111451. [CrossRef] [PubMed]
66. Choi, Y.M.; Shin, D.H.; Kim, C.-H. An Optimized Methodology to Observe Internal Microstructures of *Aloe vera* by Cryo-Scanning Electron Microscope. *Appl. Microsc.* **2016**, *46*, 76–82. [CrossRef]
67. Khuri, A.I.; Cornell, J.A. *Response Surfaces: Designs and Analyses*, 2nd ed.; CRC Taylor & Francis Group: New York, NY, USA, 1996.
68. Salman, M.; Shahid, M.; Sahar, T.; Naheed, S.; Mahmood-ur-Rahman; Arif, M.; Iqbal, M.; Nazir, A. Development of Regression Model for Bacteriocin Production from Local Isolate of Lactobacillus Acidophilus MS1 Using Box-Behnken Design. *Biocatal. Agric. Biotechnol.* **2020**, *24*, 101542. [CrossRef]
69. Mourabet, M.; El Rhilassi, A.; El Boujaady, H.; Bennani-Ziatni, M.; Taitai, A. Use of Response Surface Methodology for Optimization of Fluoride Adsorption in an Aqueous Solution by Brushite. *Arab. J. Chem.* **2017**, *10*, S3292–S3302. [CrossRef]
70. Zhang, B.; Han, X.; Gu, P.; Fang, S.; Bai, J. Response Surface Methodology Approach for Optimization of Ciprofloxacin Adsorption Using Activated Carbon Derived from the Residue of Desilicated Rice Husk. *J. Mol. Liq.* **2017**, *238*, 316–325. [CrossRef]
71. Zaheer, Z.; AbuBaker Bawazir, W.; Al-Bukhari, S.M.; Basaleh, A.S. Adsorption, Equilibrium Isotherm, and Thermodynamic Studies to the Removal of Acid Orange 7. *Mater. Chem. Phys.* **2019**, *232*, 109–120. [CrossRef]
72. Al-Zawahreh, K.; Barral, M.T.; Al-Degs, Y.; Paradelo, R. Comparison of the Sorption Capacity of Basic, Acid, Direct and Reactive Dyes by Compost in Batch Conditions. *J. Environ. Manag.* **2021**, *294*, 113005. [CrossRef]

73. Khataee, A.R.; Vafaei, F.; Jannatkhah, M. Biosorption of Three Textile Dyes from Contaminated Water by Filamentous Green Algal *Spirogyra* sp.: Kinetic, Isotherm and Thermodynamic Studies. *Int. Biodeterior. Biodegrad.* **2013**, *83*, 33–40. [CrossRef]
74. Bourikas, K.; Stylidi, M.; Kondarides, D.I.; Verykios, X.E. Adsorption of Acid Orange 7 on the Surface of Titanium Dioxide. *Langmuir* **2005**, *21*, 9222–9230. [CrossRef] [PubMed]
75. Daneshvar, E.; Kousha, M.; Sohrabi, M.S.; Khataee, A.; Converti, A. Biosorption of Three Acid Dyes by the Brown Macroalga Stoechospermum Marginatum: Isotherm, Kinetic and Thermodynamic Studies. *Chem. Eng. J.* **2012**, *195–196*, 297–306. [CrossRef]
76. Makrygianni, M.; Lada, Z.G.; Manousou, A.; Aggelopoulos, C.A.; Deimede, V. Removal of Anionic Dyes from Aqueous Solution by Novel Pyrrolidinium-Based Polymeric Ionic Liquid (PIL) as Adsorbent: Investigation of the Adsorption Kinetics, Equilibrium Isotherms and the Adsorption Mechanisms Involved. *J. Environ. Chem. Eng.* **2019**, *7*, 103163. [CrossRef]
77. Podder, M.S.; Majumder, C.B. Studies on the Removal of As(III) and As(V) through Their Adsorption onto Granular Activated Carbon/$MnFe_2O_4$ Composite: Isotherm Studies and Error Analysis. *Compos. Interfaces* **2016**, *23*, 327–372. [CrossRef]
78. Al-Ghouti, M.A.; Da'ana, D.A. Guidelines for the Use and Interpretation of Adsorption Isotherm Models: A Review. *J. Hazard. Mater.* **2020**, *393*, 122383. [CrossRef]
79. Jin, X.; Jiang, M.-Q.; Shan, X.-Q.; Pei, Z.-G.; Chen, Z. Adsorption of Methylene Blue and Orange II onto Unmodified and Surfactant-Modified Zeolite. *J. Colloid Interface Sci.* **2008**, *328*, 243–247. [CrossRef]
80. Albadarin, A.B.; Mangwandi, C. Mechanisms of Alizarin Red S and Methylene Blue Biosorption onto Olive Stone By-Product: Isotherm Study in Single and Binary Systems. *J. Environ. Manag.* **2015**, *164*, 86–93. [CrossRef]
81. Hamzeh, Y.; Ashori, A.; Azadeh, E.; Abdulkhani, A. Removal of Acid Orange 7 and Remazol Black 5 Reactive Dyes from Aqueous Solutions Using a Novel Biosorbent. *Mater. Sci. Eng. C* **2012**, *32*, 1394–1400. [CrossRef]
82. Silva, J.P.; Sousa, S.; Rodrigues, J.; Antunes, H.; Porter, J.J.; Gonçalves, I.; Ferreira-Dias, S. Adsorption of Acid Orange 7 Dye in Aqueous Solutions by Spent Brewery Grains. *Sep. Purif. Technol.* **2004**, *40*, 309–315. [CrossRef]
83. Sheshmani, S.; Ashori, A.; Hasanzadeh, S. Removal of Acid Orange 7 from Aqueous Solution Using Magnetic Graphene/Chitosan: A Promising Nano-Adsorbent. *Int. J. Biol. Macromol.* **2014**, *68*, 218–224. [CrossRef]
84. Carmalin, S.A.; Lima, E.C. Removal of Emerging Contaminants from the Environment by Adsorption. *Ecotoxicol. Environ. Saf.* **2018**, *150*, 1–17. [CrossRef]
85. Li, J.; Yu, G.; Pan, L.; Li, C.; You, F.; Xie, S.; Wang, Y.; Ma, J.; Shang, X. Study of Ciprofloxacin Removal by Biochar Obtained from Used Tea Leaves. *J. Environ. Sci.* **2018**, *73*, 20–30. [CrossRef] [PubMed]
86. Abramian, L.; El-Rassy, H. Adsorption Kinetics and Thermodynamics of Azo-Dye Orange II onto Highly Porous Titania Aerogel. *Chem. Eng. J.* **2009**, *150*, 403–410. [CrossRef]